Catalysis Science & Technology

ROYAL SOCIETY OF CHEMISTRY

PAPER

View Article Online
View Journal | View Issue

Cite this: *Catal. Sci. Technol.*, 2023, 13, 4988

Interaction of 2-propanol with predominantly SrO- and TiO_2-terminated $SrTiO_3$(100) surfaces studied by vibrational sum frequency spectroscopy†

Anupam Bera,‡[a] Denise Bullert,[a] Matthias Linke,[a] Steffen Franzka,[b] Ulrich Hagemann,[b] Nils Hartmann§[b] and Eckart Hasselbrink §*[a]

Received 3rd March 2023,
Accepted 19th June 2023

DOI: 10.1039/d3cy00310h

rsc.li/catalysis

The interaction of 2-propanol with $SrTiO_3$(100) surfaces is studied with a focus on the role of different surface terminations in the deprotonation upon adsorption. Preferential SrO and TiO_2-termination was corroborated by AFM, ARXPS and SIMS. Surface sensitive vibrational sum frequency spectroscopy (vSFS) reveals that 2-propanol predominantly adsorbs intact on SrO-terminated $SrTiO_3$(100), but is to a large extent deprotonated on TiO_2-terminated $SrTiO_3$(100). The latter is in contrast with the lack of deprotonation of 2-propanol when interacting with thin film TiO_2 as reported earlier.

1 Introduction

In the global effort to develop the faculties eventually allowing us a rational design of materials for heterogeneous catalysis, understanding the adsorption chemistry – including structure, composition and orientation of adspecies – is a key factor. This fundamental knowledge is a prerequisite for identifying the mechanistic steps underpinning how specific structural organisation leads to the reactivity and selectivity in the overall catalytic process.

Titanium dioxide (TiO_2)[1–4] and strontium titanate ($SrTiO_3$, henceforth abbreviated as STO)[5,6] are among the most studied metal-oxides in catalysis research owing to their great potential for large scale applications. In particular, redox catalytic properties of STO – a perovskite – have been intensely studied and recently reviewed[7,8] while the acid–base catalytic properties of this catalyst have been studied to a much lesser extent.[7,9] Although oxidation of alcohol species is of high industrial significance, the interaction between 2-propanol and TiO_2 and $SrTiO_3$ has received little attention. Recently, Roy and coworkers experimentally and theoretically studied the interaction of 2-propanol with pristine STO(100).[10] Furthermore, 2-propanol interacting with TiO_2(110)[11–13] and ceria(100) was reported.[14]

Complex surfaces such as the ones of mixed metal oxides exhibit a variety of surface terminations which differ in their acid–base character. Vibrational sum frequency spectroscopy (vSFS) is ideally suited to study the surface chemistry upon adsorption of a probe molecule under near ambient pressure conditions due to its surface specificity. Thus, our present effort aims to identify the role of acid–base properties in SrO and TiO_2-terminated STO(100) surfaces by comparing the adsorption behaviour of 2-propanol between these. Specifically, TiO_2 and SrO surface terminations (one aspect of the surface reconstruction) of $SrTiO_3$(100) (see Fig. 1) were achieved with the help of thermal and chemical treatments in an acidic environment.

Under real world catalytic conditions for alcohol oxidation – especially in liquid-phase catalysis – some water will always be present as it is formed as a reaction by-product. Hence,

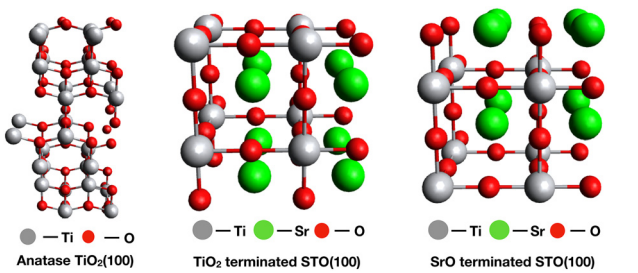

Fig. 1 Ideal surface models of anatase TiO_2(100) (left), TiO_2-terminated STO(100) (middle) and SrO-terminated STO(100) (right) 2 × 2 × 2 supercell structures.

[a] *Fakultät für Chemie, Universität Duisburg-Essen, D-45117 Essen, Germany. E-mail: Eckart.Hasselbrink@Uni-Duisburg-Essen.de; Tel: +49 201 183 3055*
[b] *Interdisciplinary Center for Analytics on the Nanoscale (ICAN), Universität Duisburg-Essen, D-47057 Duisburg, Germany*

† Electronic supplementary information (ESI) available: (i) Characterization of the samples with AFM, SIMS and ARXPS. (ii) Obtained fitting parameters for the vSF spectra. See DOI: https://doi.org/10.1039/d3cy00310h

‡ Present address: Institute of Physical Chemistry, Universität Jena, D-07743 Jena, Germany.

§ Center for Nanointegration (CENIDE), Universität Duisburg-Essen.

we aim in our study to replicate conditions characterized by an ambient atmosphere of alcohol close to its saturation vapour pressure and some residual water which sets this study apart from related ones carried out in air[15] or in UHV.[13] As a consequence, the sample surfaces will be at least partly hydroxylated because of the non-zero probability for dissociative interactions of H_2O with transition metal oxide surfaces.[16]

We have recently reported on the adsorption chemistry of 1-propanol and 2-propanol on microcrystalline thin film TiO_2.[17] No indication of deprotonation upon adsorption was detected in contrast to the results reported for methanol[18] and ethanol. In view of this background, a detailed comparative study of the adsorption properties on more complex TiO_2- and SrO-terminated surfaces would be fundamentally important to gain further insight into the underlying role of the surface's acid–base properties. However, to the best of our knowledge, no comprehensive study on adsorption selectivity by controlling the surface termination of the $SrTiO_3$(100) surface has been reported to date.

In this paper, we build on the preparation of STO(100) samples preferentially terminated by either TiO_2 or SrO.[19] We report that the propensity of deprotonation of 2-propanol when interacting with the two terminations is vastly different, with no observable deprotonation for the SrO termination and a substantial deprotonated coverage for the TiO_2 one. The latter is in contrast with an earlier report by us where 2-propanol stays intact on microcrystalline TiO films.

2 Experimental methods

2.1 Sample preparation

TiO_2 thin films of 150 nm thickness were prepared in a local optical workshop by evaporating Ti_2O_3 on glass slides. They are known to be microcrystalline and have a predominant anatase structure.[20] STO(100) surfaces were prepared by following a well-established procedure[19,21] consisting of three steps: cleaning, chemical etching and annealing. At first, the substrates which were received from MaTeck were cleaned in acetone, ethanol and 2-propanol using an ultrasonic bath at room temperature for 5 min in each solvent to remove any organic contaminants. In the 2nd step, a buffered hydrofluoric acid solution with pH 4.5 was utilized to remove any basic SrO by dipping into the solution for 30 s to obtain a TiO_2-terminated surface. In the 3rd step, the etched samples were baked at 1000 °C in air for 90 min to obtain a TiO_2-terminated surface with large flat terraces.[22] Alternatively, the baking temperature was increased to 1200 °C and the duration extended to 72 h in order to obtain a SrO-terminated surface due to exdiffusion of Sr from the bulk. As a reference, a sample was also studied, which was prepared starting from the as-received crystal and skipping the annealing step, further referred to as the reference sample. Before recording any vSF spectra, the samples were further cleaned utilizing a two-stage cleaning process: i) exposure to an oxygen plasma (0.4 mbar, 15–30 min) and ii) after mounting in the spectroscopy cell, they were exposed to UV irradiation generated by a Xe lamp (Osram, XBO 150 W/1) in the presence of an oxygen atmosphere (100–200 mbar, 2–5 h).

Anhydrous 2-propanol (99.5%) was obtained from Sigma Aldrich and used without further purification.

2.2 Secondary ion mass spectrometry

Time-of-flight secondary ion mass spectrometry (ToF-SIMS) was employed using a TOF.SIMS 5-100 (IONTOF). For surface analysis, the beam from a Bi^+ primary ion gun operated in spectrometry mode at 30 kV was scanned in random mode at a field size of 500 × 500 μm^2 and a digital raster of 256 × 256 pixels. Complementary measurements were also carried out at 15 kV. Charge compensation was ensured by employing a low energy electron flood gun. The analyzer was operated in positive polarity and corrected in order to compensate for surface potential shifts. The typical surface sensitivity at these parameters corresponds to an information depth of ≤1 nm. Parameters for dual beam depth profiling were chosen in order to ensure high sputter rate ratios, low transient widths, and high vertical resolution. For analysis, the Bi^+ primary ion gun in this case was operated at 15 kV, a field size of 100 × 100 μm^2, a digital raster of 128 × 128 pixels and otherwise unchanged parameters (*cf.* above, also considering charge compensation and analyzer settings). Noninterlaced sputtering was performed using a Xe^+ source operated at 500 V and a sputter field size of 400 × 400 μm^2. After each analysis cycle, a layer of the material was removed in a subsequent sputter cycle at a frame ratio of 1 : 1. Some depth profiling measurements were also carried out operating the primary ion gun at 30 kV and employing a higher analysis and sputter frame ratio of 1 : 10. ToF-SIMS measurements generally were carried out at 3–5 different positions in order to check for surface heterogeneities. Depths of final sputter craters created with long sputter times were determined from profilometry measurements with a Dektak XT (Bruker) and a Sensofar S-neox (Sensofar). An apparent sputter rate of 0.037 nm s^{-1} was calculated taking these depth values into account assuming a constant erosion rate.

2.3 Atomic force microscopy

Surface topography was investigated by atomic force microscopy (AFM), performed in air (RH = 20–30%, T = 21 °C) using a Bruker Dimension Icon AFM in tapping mode. The typical scan rate was 1 Hz and 512 samples per line were acquired. RTESPA cantilevers (nom. resonant frequency: 300 kHz, nom. spring constant: 40 N m^{-1}, nom. tip radius: 8 nm, Bruker) were used. Image analysis was performed using NanoScope Analysis 1.9 (Bruker). The images were flattened and eventually low-pass filtered to remove high frequency noise.

2.4 Angle resolved X-ray photoelectron spectroscopy

For angle resolved X-ray photoelectron spectroscopy (ARXPS), a VersaProbe II (Physical Electronics) with a microfocused X-ray source (Mg Kα = 1486.6 eV) was used.

2.5 Vibrational sum frequency spectroscopy

Vibrational sum frequency spectroscopy is based on a non-linear 3-wave mixing process, the details of which were discussed in detail by several authors.[23,24] A scanning vSF spectrometer with approx. 12 cm^{-1} resolution was used (Ekspla PL2231 and PG501DFG) that utilizes wavelength tuneable IR pulses and 532 nm light pulses of 25 ps duration at a repetition rate of 25 Hz for upconversion. Pulse energies of 280 μJ (532 nm) and 10–30 μJ (IR) were utilized. For every data point, typically 300 laser pulses were sampled and averaged. To correct the daily variance in laser performance, the vSF signal from a Au surface was obtained as a calibration reference before recording a spectrum.

The experimental set-up was described in detail elsewhere (Fig. 2).[18] The samples were mounted in a home-built compact cell (63 mm inner diameter) which allowed for the preservation of a rough vacuum. 50 mbar of 2-propanol, which is close to its saturation pressure, was admitted, utilizing an evaporator. The laser beams enter and the signal leaves the cell through a MgF_2 window. The IR and upconversion light beams were directed at the sample at incident angles of 53° and 62°, respectively. And the SF signal reflected from the top surface was recorded.

The spectra were fitted using the following, established expressions:[25,26]

$$I^{\mathrm{SFS}}(\omega_{\mathrm{IR}}) \propto \left| \left|\chi^{(2)}_{\mathrm{NR}}\right| + \sum_i e^{i\xi_i} \frac{A_i}{\omega_{\mathrm{IR}} - \omega_i + i\Gamma_i} \right|^2, \quad (1)$$

where $\chi^{(2)}_{\mathrm{NR}}$ represents the 2nd order susceptibility of the substrate electronic system leading to a non-resonant background. A_i, ω_i and Γ_i are the vSF line strength, the position and the width (HWHM) of the ith vibrational resonance, respectively. ω_{IR} is the angular frequency of the incident IR light.

These parameters are real numbers and A_i has a positive value in our model. ξ_i is the relative phase of the response of each individual line with respect to the non-resonant background. For the ssp polarization combination, the responses of symmetric stretches and anti-symmetric ones of CH stretching modes have a phase difference of π. For the ppp polarization combination, that difference is treated as a fitting parameter.[27] We choose to constrain the fitting such that all symmetric modes share a common phase, while in-plane and out-of-plane anti-symmetric modes share different ones in order to limit the number of free parameters.

The surface density of an adsorbed species N_i can be inferred from the A_i parameters derived from the fit to a spectrum as they are connected according to the following expression:[28]

$$A_i = N_i \langle a_i \rangle_f = N_i \int a_i f(\Omega) \mathrm{d}\Omega, \quad (2)$$

where N_s is the surface density of molecules, a_i is the non-linear molecular hyperpolarizability strength associated with the ith vibrational resonance, $\langle\rangle_f$ indicates an average with respect to the orientation distribution function $f(\Omega)$ and Ω denotes the set of three Euler angles.

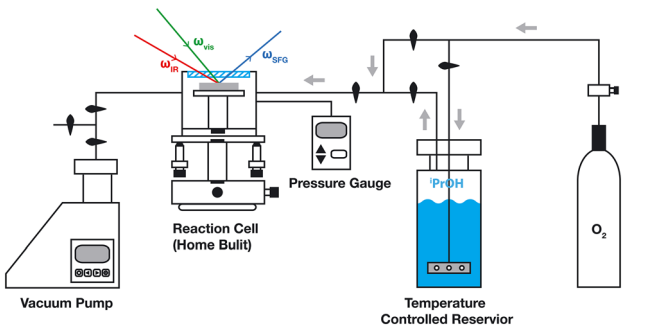

Fig. 2 Experimental set-up. The sample is housed in a home built flow cell that is evacuated by a membrane pump to mbar levels. 2-Propanol is introduced into the cell from a temperature controlled reservoir. The laser beams enter and the signal light left the cell through a MgF_2 window. Oxygen is available for sample cleaning by UV light exposure in an atmosphere of that gas.

3 Results and discussion

3.1 Sample characterization

Experiments were conducted using i) a reference STO(100) substrate and ii) either preferentially TiO_2- or SrO-terminated samples. Moreover, we refer to the vSF spectra obtained in an earlier study using iii) TiO_2 nanocrystalline thin films (*ca.* 150 nm) of predominantly anatase structure deposited on glass substrates.[17] The success of the preparation of one particular surface termination was verified by ToF-SIMS and XPS. Noteworthily, however, both ToF-SIMS and grazing-incidence XPS surface analysis sample the surface well beyond the very top layer. The surface morphology was studied using AFM.

All three types of STO samples, referred to as the TiO_2-terminated sample, SrO-terminated sample and reference sample, were analyzed by ToF-SIMS after carrying out the 2 or 3 initial preparation steps discussed above. Thereafter, the samples were handled in air and introduced into vacuum. As matrix effects are well known to complicate the ToF-SIMS analysis of oxidic materials, the analytical results obtained on the reference sample here are used as a point of reference. Following this approach, the comparison of respective ion intensity ratios, such as the Ti^+/Sr^+ intensity ratios presented in Fig. 3, is considered to semi-quantitatively reflect corresponding changes of the relative concentration ratios. As expected, the Ti^+/Sr^+ intensity ratio is significantly higher on the TiO_2 terminated sample and the Ti^+/Sr^+ intensity ratio is significantly lower on the SrO terminated sample when compared with the values obtained on the reference sample. This suggests that the Ti^+/Sr^+ concentration ratio indeed is higher on the TiO_2 terminated sample and lower on the SrO terminated sample.

Fig. 4 shows the corresponding data from ToF-SIMS depth profiling. Again we use the analytical data obtained on the reference sample, *i.e.*, the Ti^+_{Ref}/Sr^+_{Ref} intensity ratio, as

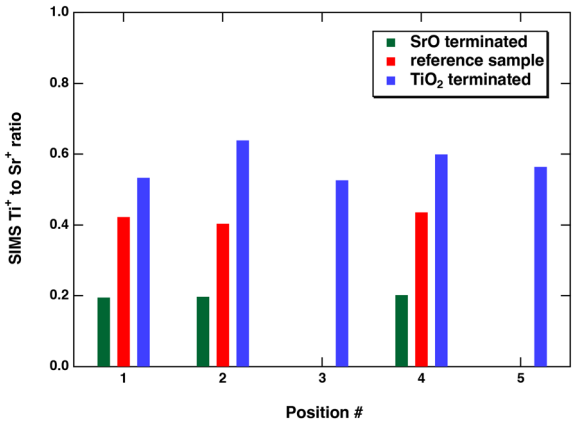

Fig. 3 Ratios of the Ti^+ to Sr^+ signals obtained in ToF-SIMS for the STO(100) samples prepared with different preferential terminations and the reference sample. The measurement was carried out at up to 5 different lateral positions. For positions 1 to 3, an ion energy of 30 keV was used and for positions 4 and 5, 15 keV.

reference for normalization (*cf.* ESI† for data and discussion of Ti^+/Sr^+ depth profiles for all three types samples). Noteworthily, at the beginning of the measurements, sputter yields and ionization probabilities are stabilizing. Also, residual surface contaminants from sample storage and transport in ambient air are removed in the first few sputtering cycles. This impedes a detailed quantitative analysis in this transient region with a depth of <1 nm.

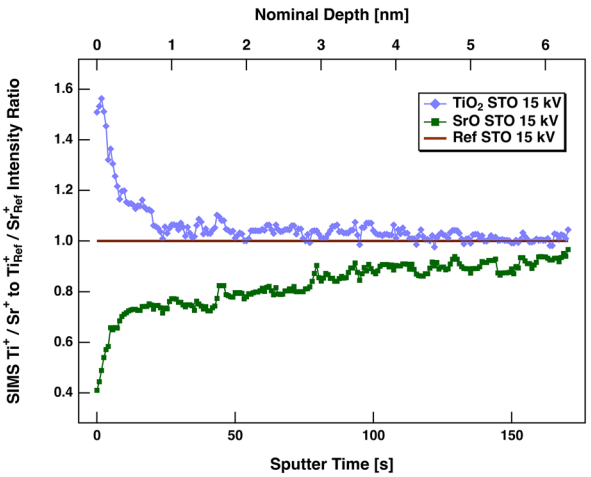

Fig. 4 Normalized depth profiles in SIMS obtained for the STO(100) samples with preferential TiO_2 and SrO terminations, respectively. Shown is the Ti^+/Sr^+ intensity ratio normalized to the Ti^+_{Ref}/Sr^+_{Ref} intensity ratio obtained for the STO(100) reference sample, which is represented by the horizontal line at an intercept of 1. Prior to normalization, the depth profiles are smoothened using a 5 point median filter. The bottom axis shows the sputtering time, while the top axis shows the nominal sputter depth taking a sputtering rate of ≈0.037 nm s^{-1} into account. In the beginning of the measurement, ionization rates are stabilizing. After around 150 s –corresponding to a depth of 5.5 nm – all depth profiles approach the ratio corresponding to the bulk material.

Clearly, however, the normalized data here point to an increased Ti/Sr concentration ratio in the near-surface region of the TiO_2 terminated sample before a constant ratio as in the bulk at a depth of 5–6 nm is reached. Also, even more pronounced, the data indicate a reduced Ti/Sr concentration ratio in the near-surface region of the SrO terminated sample, again approaching a constant ratio in the bulk at a depth of 5–6 nm.

Complementary AFM measurements (for a detailed discussion see ESI†) reveal a rearrangement and ordering of the sample surface structure upon annealing.

The ToF-SIMS data are corroborated by additional X-ray photoemission spectroscopy (XPS) measurements carried out at grazing incidence (Fig. 5). For the discussion, we use the ratio of the Ti signal (E_{bind} = 458.5 eV) to the sum of two Sr signals, namely the one from $SrTiO_3$ and the one from SrO split by 0.6 eV and located at around 133 eV. The signals show a strong dependence on the emission angle. For the emission along the surface normal, the observed ratios are only a little different for the three samples. However, towards the grazing emission angle, the ratios progressively diverge as this technique progressively probes a smaller depth into the sample. The ratio decreases for the SrO-terminated sample and increases somewhat less pronounced for the other two, consistent with the expected predominance of Sr over Ti or *vice versa* in the near surface region. Notwithstanding the fact that at the smallest emission angle the data values only span the range from 1 to 0.5, it is worth noting that due to the extended information depth, these values could well point to a significantly larger enrichments of Ti or alternatively Sr at the surface. In view of this mismatch between the information depth at the smallest emission angle of 10° estimated as 1.5 nm and the size of the STO unit cell of 3.91 Å,[29] the data are consistent with a near exclusive Sr termination in one case and strongly preferential Ti termination in the other. Noteworthily, the XPS data reveal a

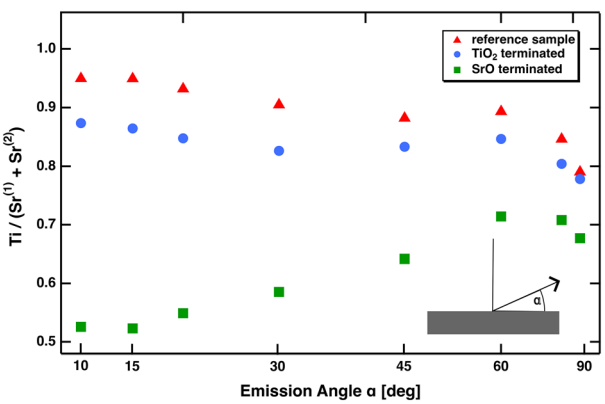

Fig. 5 Ti (E_{bind} = 458.5 eV) ARXPS signal in relation to the sum of Sr signals at binding energies of 133 eV ($SrTiO_3$) and 133.6 eV (SrO) in angle resolved X-ray photoemission spectroscopy as a function of emission angle α. Noteworthily, the *x*-axis is sin-scaled. Thus, the depth into the sample contributing to the signal should linearly increase from left to right.

higher Ti/Sr ratio for the reference sample in comparison to the TiO_2-terminated sample. This is in contrast with the ToF-SIMS results. The difference, however, is comparatively small and might well result from certain analytical complications and differences of the two techniques. The ToF-SIMS analysis could still be affected by matrix effects, for example. Also, a higher surface sensitivity of the ToF-SIMS analysis could explain the difference.

3.2 Surface layer vibrational spectroscopy

The vSF spectrum of 2-propanol in the C–H stretching region was discussed by us before when studying its interaction with TiO_2 (Fig. 6).[17] With increasing alkyl chain length, the spectra of alcohols become congested as a larger number of C–H modes are to be considered, which often overlap and for which multiple Fermi resonances are possible. The first assignment of the features observed in the vSF spectrum of 2-propanol was made by Wang *et al.*[30,31] and later adopted by Kataoka.[32] Yu *et al.* revised some of the earlier assignments based on a higher resolution Raman study of gas and liquid phase 2-propanol.[33] At least four modes are to be expected: namely the CH_3 symmetric-stretch, r^+, and a related Fermi resonance with the overtone of the degenerated bending mode, r^+_{FR}, the CH_3 anti-symmetric stretch, r^-, and a methine CH stretching mode. The latter is split into two, due to differing interactions with the OH-group in the *gauche*- and *trans*-conformation of the methine CH-bond. Furthermore, a combination mode of the two was clearly identified by us when recording the spectra of $CD_3CHOHCD_3$.[17] The sps spectrum allows us to clearly identify the r^- mode at 2972 cm^{-1}. More precisely, this is the out-of-plane mode. Meanwhile, the in-plane mode, located about 12 cm^{-1} higher in the wavenumber, carries less amplitude and we did not find it absolutely necessary to include it in every fit to a spectrum. In that case, we refrained from including it as the then larger number of parameters would only increase their arbitrariness. The modes at 2880 and 2940 cm^{-1} are predominant in the ssp spectrum and are assigned to the r^+ mode and its Fermi resonance. Which of the two modes is the r^+ one and which the Fermi resonance is debated in the literature. Yu *et al.* reported two further Fermi resonances, located at 2917 and 2933 cm^{-1} which we are not able to identify in our spectra. The conclusion is that the modes at 2880 and 2940 cm^{-1} overlap with the ones from the methine group. Hence, we treated them as one feature each in the fitting function, which should be possible as all these are symmetric modes which are anyway to some extent coupled. For this reason, we refrained from evaluating the amplitudes of these modes and only used a mode placed at 2916 cm^{-1} in the fit function as an indication of the contribution from the methine mode.

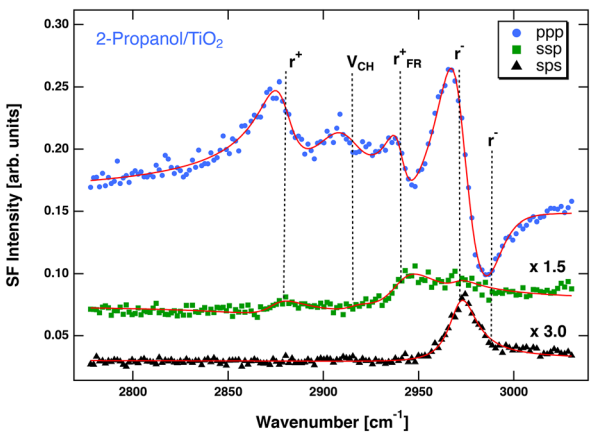

Fig. 6 vSF spectra of a microcrystalline TiO_2 thin film surface exposed to 50 mbar of 2-propanol. Spectra were obtained for the ppp, ssp and sps polarization combinations. The ppp spectrum is severely influenced by a non-resonant background. The solid lines represent fits to the data. The dashed lines indicate the centre positions of the bands identified. Noteworthily, although the *y*-axis is scaled in arbitrary units, these are identical in all figures of the vSF spectra. Adopted from ref. 17.

A detailed orientation analysis following the approach introduced by Kataoka and Cremer[32] and adapted by Doughty *et al.*[14] suggests that the symmetry axis of the 2-propyl group is directed nearly in-plane with the surface but that one of the two methyl groups points more upwards, while the other points more towards the surface.[17] The C–O bond points then at an angle of 122° with respect to the normal towards the surface allowing the H in the OH group to come close to the surface. However, the determination of definite orientation angles in systems as the ones studied here has to be taken with a grain of salt, as recent *ab initio* molecular dynamics simulations by us[34] demonstrated that the physisorbed molecule carries out large amplitude rotational motions which renders the notion of a preferred geometry at least questionable.

The spectrum of 2-propanol adsorbed on thin film TiO_2 can very well be fitted without the need to assume that a fraction of the adsorbate is deprotonated. The deprotonated species generally exhibits a shift of all modes to smaller wavenumbers by about 20–30 cm^{-1} as was observed when studying adsorbed methanol and ethanol on TiO_2.[17,18,35] Hence, the lack of this spectral signature suggests that the extent of deprotonation for 2-propanol is too small to detect, pointing at a too low reactivity despite the fact that the O–H moiety is located close to the surface.

Surprisingly, the spectrum obtained for the predominantly TiO_2-terminated STO(100) surface suggests a different chemistry (Fig. 7). For our purpose here, it needs to be noted that in particular the ppp spectrum can only be understood when assuming that a second species is present with similar bands but offset by about 21 cm^{-1}. In particular, the feature at 2858 cm^{-1} is not present in the spectrum of the TiO_2 sample. It is identified as the r^+ mode of the deprotonated species, and thereby unambiguously indicating its presence in larger abundance. This interpretation is consistent with earlier studies on methanol[18,35] and higher alcohol deprotonation.[17] Apart from this finding, the coarse difference between the spectra is due to the non-resonant

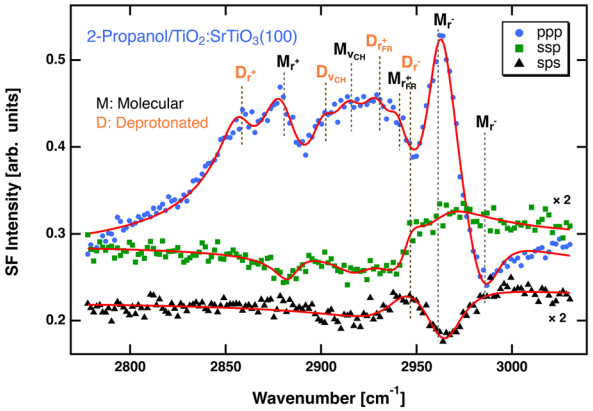

Fig. 7 vSF spectra of a TiO_2-terminated STO(100) surface exposed to 50 mbar of 2-propanol. Spectra were obtained for the ppp, ssp and sps polarization combinations. The ppp spectrum is severely influenced by a non-resonant background. The solid lines represent fits to the data. The dashed vertical lines indicate the centre positions of the bands identified. Features assigned to modes from the intact molecular species are labeled with M, and the ones assigned to the deprotonated species with D.

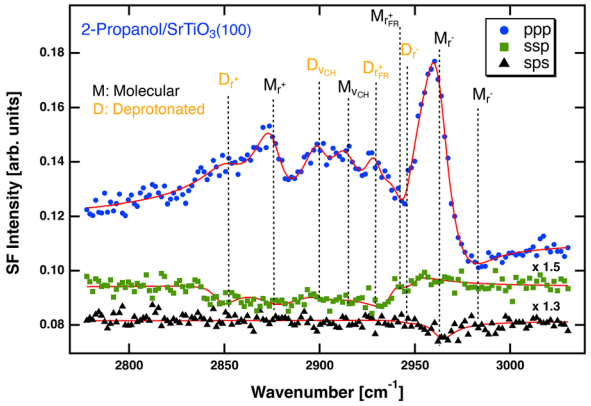

Fig. 9 vSF spectra of a reference STO(100) surface exposed to 50 mbar of 2-propanol. Spectra were obtained for the ppp, ssp and sps polarization combinations. The ppp spectrum is severely influenced by a non-resonant background. The solid lines represent fits to the data. The dashed vertical lines indicate the centre positions of the bands identified. Features assigned to modes from the intact molecular species are labeled with M, and the ones assigned to the deprotonated species with D.

background that is by a factor 1.2 larger for the TiO_2-terminated sample. While the relative phases between the modes are similar for TiO_2 and TiO_2–STO, they are offset by 0.6 rad with respect to the non-resonant background. This results in the r^- mode appearing as a dip in the sps spectrum rather than a peak.

The spectrum obtained for the predominantly SrO-terminated surface differs substantially (Fig. 8). Due to the different dielectric response of the surface, the molecular modes exhibit a different phase with respect to the non-resonant background. However, the spectrum shows no indication of deprotonated 2-propanol. Note the lack of the feature at 2855 cm^{-1} that was indicative in the case of the spectrum of the TiO_2-terminated sample.

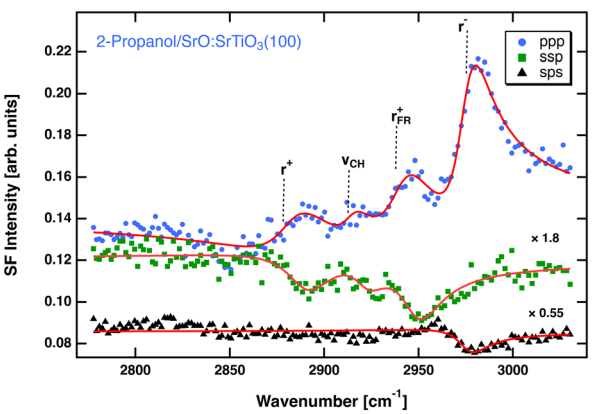

Fig. 8 vSF spectra of a SrO-terminated STO(100) surface exposed to 50 mbar of 2-propanol. Spectra were obtained for the ppp, ssp and sps polarization combinations. The ppp spectrum is severely influenced by a non-resonant background. The solid lines represent fits to the data. The dashed vertical lines indicate the centre positions of the bands identified.

Furthermore, it is worth noting that the spectra obtained from the reference sample (Fig. 9) also indicate the presence of the deprotonated species. Overall, its structure is rather similar to that of TiO_2–STO but with less pronounced features from the deprotonated species, indicating a smaller abundance. This finding is perhaps not surprising as SIMS indicated that the additional Ti enrichment at the surface after the milder baking procedure is only about 10%.

Hence, we are left with the puzzling observation that 2-propanol is deprotonated on the reference sample and the predominantly TiO_2-terminated one, but not on the TiO_2 thin film nor the predominantly SrO-terminated STO(100) sample.

There are several lines of thought to address this question: this observation is consistent with Sr being a weaker Lewis acid than Ti as reported by Chapleski *et al.*[10] According to their results, TiO_2- and SrO-terminated surfaces differ in Lewis-acid character because Ti carries a higher partial charge than Sr with the consequence that 2-propanol binds more strongly by 0.49 eV on STO(100) terminated with TiO_2 than on STO(100) terminated with SrO. In another recent work,[9] adsorption microcalorimetry was utilized to characterize the surfaces of $SrTiO_3$ with CO_2 and NH_3. In general, the result showed that SrO-terminated STO(100) has more basic sites and fewer acidic sites when compared with TiO_2-termination, which is consistent with the higher Sr/Ti ratio on the SrO–STO sample. However, the strength of the basic or acid sites does not directly correlate with the density of the Ti sites. This finding might suggest that Sr–O or Ti–O sublayers work synergistically to tune the basic/acid properties of the surface.

Generally, the stronger binding goes along with a larger activation of the OH bond, as the strongest interaction of the intact molecule with the surface is *via* the oxygen atom. As a

result, 2-propanol's O–H bond dissociation energies out of the molecularly bound state are higher on the SrO-terminated surfaces than on the TiO_2-terminated surfaces. However, it is interesting to note that 2-propanol remains undissociated on thin-film TiO_2. Thus, it is most likely an electronic effect that increases Ti′s Lewis acidity in the presence of Sr in STO(100). A more in-depth investigation is needed to confirm this hypothesis.

However, there is no justification for a monotonous relationship between the binding energy of the molecular species and the propensity to deprotonate. As much as the higher binding energy goes along with the weakening of the OH bond, *i.e.* an elongation of the bond, it stabilizes the system in this state. In other words, the larger binding energy may go along with a larger activation energy towards the transition state. It is at least conceivable that there exists an intermediate regime of binding energies in which the OH bond is elongated but at the same time the barrier towards deprotonation is not prohibitively high. In this speculative interpretation, the surface of STO(100) with predominant TiO_2 termination might just have the right energetics, while the binding is too large in the case of the TiO_2 films and the OH bond activation too small in the case of the SrO-terminated STO(100) surface.

A further aspect to address in search for the underlying reason is the surface morphology that was characterized by atomic force microscopy in this work (AFM). However, images show in either case large rather flat terraces with single unit cell height steps in the case of TiO_2–STO and several cell height steps in the case of SrO–STO, and straight step-edges in either case (see the ESI†). Hence, the surface morphology may play some role but will not be the decisive factor explaining the different reactivity. However, it may be worth noting that Bondarchuk *et al.*[12] reported that disrupting the long range order, *e.g.* by mild sputtering, inhibited 2-propanol reacting at low temperatures on TiO_2(110). Nevertheless, the geometric difference between the lattices of TiO_2 and TiO_2-terminated STO may cause slight differences in the energetics of the reaction path for 2-propanol deprotonation. Moreover, it must be kept in mind that these experiments were deliberately carried out in a residual atmosphere containing substantial amounts of water vapour in order to resemble the conditions in a real reactor. As a consequence, the sample surface will be largely hydroxylated. No detailed information that would allow the differences of hydroxylation to be quantified for the differently terminated surfaces is available. However, a sufficient number of non-hydroxylated surface oxygen sites are a prerequisite for the conversion of physisorbed 2-propanol to the deprotonated adspecies. In this context, it may be noteworthy that we observed in SIMS a larger abundance of OH-containing species for the SrO-terminated substrate than for the other substrates (see the ESI† for details). It will take further efforts using theory and *in situ* surface characterisation to come up with answers to these open questions.

4 Conclusion

At room temperature, we found that 2-propanol's adsorption properties depend on the different terminations of STO(100) surfaces by surface sensitive vibrational sum frequency spectroscopy (vSFS). The extent of deprotonation of 2-propanol follows the earlier established surface acidity order of the perovskites STO(100).[9,10] The Lewis acidity and extent of deprotonation are as follows: SrO–STO(100) (negligible Lewis acidity) < off-the-shelf STO(100) < TiO_2–STO(100).[9] A comparison of thin film TiO_2 with TiO_2-terminated STO(100) indicates that Sr in STO(100) increases Ti′s Lewis acidity.

Data availability

The data from vSF spectroscopy shown in Fig. 6–9 are available from the Zenodo data depository.[36]

Author contributions

Anupam Bera: conceptualization, methodology, investigation (vSFS), resources, validation, formal analysis, writing – original draft, and visualization. Denise Bullert: investigation (vSFS). Matthias Linke: formal analysis. Steffen Franzka: investigation (AFM) and formal analysis.: Ulrich Hagemann: investigation (ARXPS) and formal analysis. Nils Hartmann: investigation (SIMS) and formal analysis. Eckart Hasselbrink: conceptualization, writing – reviewing and editing, visualization, supervision, project administration, and funding acquisition.

Conflicts of interest

There are no conflicts to declare.

Acknowledgements

This work was funded by the Deutsche Forschungsgemeinschaft (DFG, German Research Foundation) – Project-ID 388390466 – CRC/TRR 247 "Heterogeneous Oxidation Catalysis in the Liquid Phase". Support from the Interdisciplinary Center for Analytics on the Nanoscale (ICAN) of the University of Duisburg-Essen, a DFG funded core facility (DFG resources reference: RI_00313, project no. 233512597 and 324659309), is gratefully acknowledged. We thank Martin Jerman for making the TiO_2 substrates available to us. We have profited from valuable discussions with Sharani Roy.

Notes and references

1 A. Honda and K. Fujishima, *Nature*, 1972, **238**, 37–38.
2 Q. Guo, C. Zhou, Z. Ma, Z. Ren, H. Fan and X. Yang, *Chem. Soc. Rev.*, 2016, **45**, 3701–3730.
3 A. L. Linsebigler, G. Lu and J. T. Yates Jr, *Chem. Rev.*, 1995, **95**, 735–758.
4 H. Chen, C. E. Nanayakkara and V. H. Grassian, *Chem. Rev.*, 2012, **112**, 5919–5948.

5 J. M. P. Martirez, S. Kim, E. H. Morales, B. T. Diroll, M. Cargnello, T. R. Gordon, C. B. Murray, D. A. Bonnell and A. M. Rappe, *J. Am. Chem. Soc.*, 2015, **137**, 2939–2947.
6 J. Mavroides, J. Kafalas and D. Kolesar, *Appl. Phys. Lett.*, 1976, **28**, 241–243.
7 S. Royer, D. Duprez, F. Can, X. Courtois, C. Batiot-Dupeyrat, S. Laassiri and H. Alamdari, *Chem. Rev.*, 2014, **114**, 10292–10368.
8 P. Granger, V. I. Parvulescu, S. Kaliaguine and W. Prellier, *Perovskites and related mixed oxides: concepts and applications*, John Wiley & Sons, 2015.
9 F. Polo-Garzon, S.-Z. Yang, V. Fung, G. S. Foo, E. E. Bickel, M. F. Chisholm, D.-E. Jiang and Z. Wu, *Angew. Chem.*, 2017, **129**, 9952–9956.
10 R. C. Chapleski, A. U. Chowdhury, K. R. Mason, R. L. Sacci, B. Doughty and S. Roy, *Phys. Chem. Chem. Phys.*, 2021, **23**, 23478–23485.
11 Z. Zhang, O. Bondarchuk, J. White, B. Kay and Z. Dohnálek, *J. Am. Chem. Soc.*, 2006, **128**, 4198–4199.
12 O. Bondarchuk, Y. K. Kim, J. M. White, J. Kim, B. D. Kay and Z. Dohnalek, *J. Phys. Chem. C*, 2007, **111**, 11059–11067.
13 J. Kräuter, L. Mohrhusen, F. Waidhas, O. Brummel, J. Libuda and K. Al-Shamery, *J. Phys. Chem. C*, 2021, **125**, 3355–3367.
14 B. Doughty, S. G. Srinivasan, V. S. Bryantsev, D. Lee, H. N. Lee, Y.-Z. Ma and D. A. Lutterman, *J. Phys. Chem. C*, 2017, **121**, 14137–14146.
15 S. Tan, M. B. Gray, M. K. Kidder, Y. Cheng, L. L. Daemen, D. Lee, H. N. Lee, Y.-Z. Ma, B. Doughty and D. A. Lutterman, *ACS Catal.*, 2017, **7**, 8118–8129.
16 F. Fasulo, G. Piccini, A. B. Muñoz-García, M. Pavone and M. Parrinello, *J. Phys. Chem. C*, 2022, **126**, 15752–15758.
17 A. Bera, D. Bullert, M. Linke and E. Hasselbrink, *J. Phys. Chem. C*, 2021, **125**, 7721–7727.
18 A. Bera, D. Bullert and E. Hasselbrink, *J. Phys. Chem. C*, 2020, **124**, 16069–16075.
19 R. Bachelet, F. Sánchez, F. J. Palomares, C. Ocal and J. Fontcuberta, *Appl. Phys. Lett.*, 2009, **95**, 141915.
20 M. Jerman and D. Mergel, *Thin Solid Films*, 2007, **515**, 6904–6908.
21 F. Gellé, R. Chirita, D. Mertz, M. V. Rastei, A. Dinia and S. Colis, *Surf. Sci.*, 2018, **677**, 39–45.
22 R. Atif, *Appl. Phys. A: Mater. Sci. Process.*, 2020, **127**, 111.
23 A. G. Lambert, P. B. Davies and D. J. Neivandt, *Appl. Spectrosc. Rev.*, 2005, **40**, 103–145.
24 C. S. Tian and Y. R. Shen, *Surf. Sci. Rep.*, 2014, **69**, 105–131.
25 M. Buck and M. Himmelhaus, *J. Vac. Sci. Technol., A*, 2001, **19**, 2717–2736.
26 F. Vidal and A. Tadjeddine, *Rep. Prog. Phys.*, 2005, **68**, 1095–1127.
27 N. Ji, V. Ostroverkhov, C.-Y. Chen and Y.-R. Shen, *J. Am. Chem. Soc.*, 2007, **129**, 10056–10057.
28 X. Wei, X. Zhuang, S.-C. Hong, T. Goto and Y. R. Shen, *Phys. Rev. Lett.*, 1999, **82**, 4256–4259.
29 E. N. Maslen, N. Spadaccini, T. Ito, F. Marumo and Y. Satow, *Acta Crystallogr., Sect. B: Struct. Sci.*, 1995, **51**, 939–942.
30 R. Lu, W. Gan, B.-H. Wu, Z. Zhang, Y. Guo and H.-F. Wang, *J. Phys. Chem. B*, 2005, **109**, 14118–14129.
31 H.-F. Wang, W. Gan, R. Lu, Y. Rao and B.-H. Wu, *Int. Rev. Phys. Chem.*, 2005, **24**, 191–256.
32 S. Kataoka and P. S. Cremer, *J. Am. Chem. Soc.*, 2006, **128**, 5516–5522.
33 Y. Yu, Y. Wang, N. Hu, K. Lin, X. Zhou and S. Liu, *J. Raman Spectrosc.*, 2014, **45**, 259–265.
34 A. H. Omranpoor, A. Bera, D. Bullert, M. Linke, S. Salamon, S. Webers, H. Wende, E. Hasselbrink, E. Spohr and S. Kenmoe, *J. Chem. Phys.*, 2023, **158**, 164703.
35 C.-Y. Wang, H. Groenzin and M. J. Shultz, *J. Phys. Chem. B*, 2004, **108**, 265–272.
36 A. Bera, D. Bullert and E. Hasselbrink, *Zenodo data depository*, 2023, DOI: **10.5281/zenodo.7645699**.